Gravity-independent Rock-climbing Robot and a Sample Acquisition Tool with Microspine Grippers

Aaron Parness and Mathew Frost
NASA Jet Propulsion Laboratory, California Institute of Technology, Pasadena, California 91109
e-mail: Aaron.Parness@jpl.nasa.gov, Mathew.A.Frost@jpl.nasa.gov
Nitish Thatte
Carnegie Mellon University, Pittsburgh, Pennsylvania 15213
e-mail: nitisht@andrew.cmu.edu
Jonathan P. King
Ohio State University, Columbus, Ohio 43210
e-mail: king.1371@buckeyemail.osu.edu
Kevin Witkoe
University of Idaho, Moscow, Idaho 83844
e-mail: kwitkoe@comcast.net
Moises Nevarez
University of Southern California, Los Angeles, California 90089
e-mail: moisesne@usc.edu
Michael Garrett, Hrand Aghazarian, and Brett Kennedy
NASA Jet Propulsion Laboratory, California Institute of Technology, Pasadena, California 91109
e-mail: Michael.S.Garrett@jpl.nasa.gov, haghazar@jpl.nasa.gov, bkennedy@jpl.nasa.gov

Received 5 December 2012; accepted 12 July 2013

A rock-climbing robot is presented that can free climb on vertical, overhanging, and inverted rock faces. This type of system has applications to extreme terrain on Mars or for sustained mobility on microgravity bodies. The robot grips the rock using hierarchical arrays of microspines. Microspines are compliant mechanisms made of sharp hooks and flexible elements that allow the hooks to move independently and opportunistically grasp roughness on the surface of a rock. This paper presents many improvements to early microspine grippers, and the application of these new grippers to a four-limbed robotic system, LEMUR IIB. Each gripper has over 250 microspines distributed in 16 carriages. Carriages also move independently with compliance to conform to larger, cm-scale roughness. Single gripper pull testing on a variety of rock types is presented, and on rough rocks, a single gripper can support the entire mass of the robot (10 kg) in any orientation. Several sensor combinations for the grippers were evaluated using a smaller test-gripper. Rock-climbing mobility experiments are also described for three characteristic gravitational orientations. Finally, a sample acquisition tool that uses one of the robot's grippers to enable rotary percussive drilling is shown.

1. INTRODUCTION

The rock-climbing robot described here (see Figure 1) utilizes a unique technology, namely microspines (Asbeck et al., 2006b), which enable gravity-independent mobility on rocky surfaces including cliff faces, lava tubes (including the ceiling), and in microgravity environments such as the surfaces of near Earth asteroids. Microspines were invented at Stanford University in 2004 (Asbeck et al., 2005), and through the last nine years of development they have evolved into a mature technology that has been demonstrated on several climbing robots (Asbeck et al., 2006a; Kim et al., 2005; Spenko et al., 2008), in the landing gear of an unmanned air vehicle (Desbiens et al., 2010, 2011), and in human climbing paddles (Parness and DiscoveryChannel, 2009). A microspine consists of one or more steel hooks embedded in a rigid frame with a compliant suspension system made of elastic flexures or spring elements. By arraying tens or hundreds of microspines, large loads can be supported and shared between many attachment points. Since each microspine has its own suspension structure, it can stretch and drag relative to its neighbors to find a suitable asperity to grip. Microspines can attach to both convex and concave

Direct correspondence to: Aaron Parness, Aaron.Parness@jpl.nasa.gov

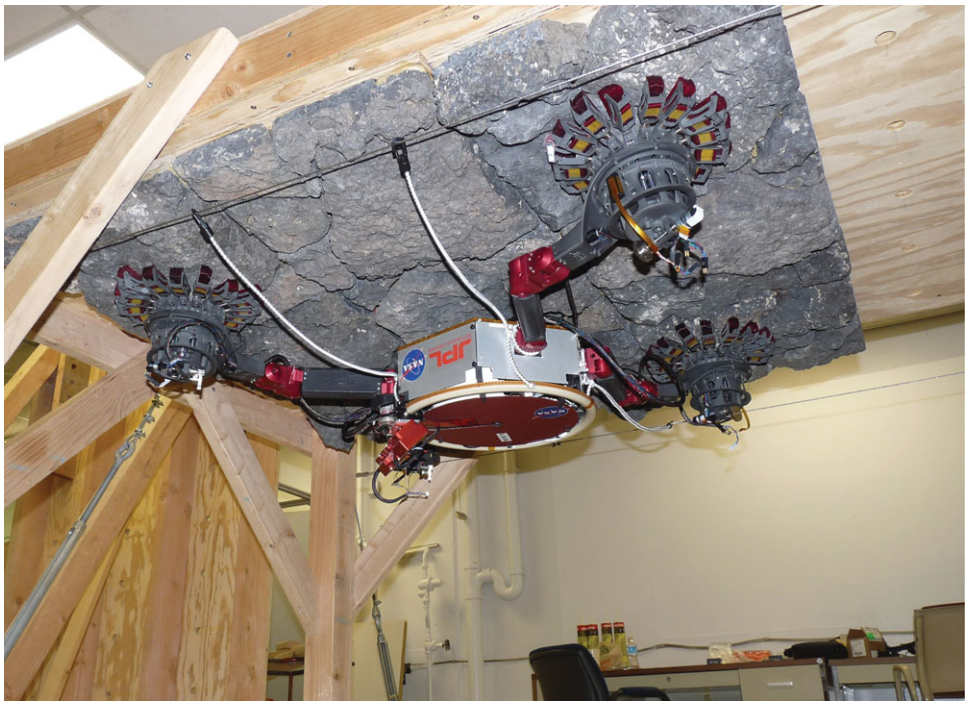

Figure 1. The LEMUR IIB robot with microspine grippers during an inverted free-climbing experiment on vesicular basalt rock.

asperities such as pits, protrusions, and sloped rock faces (Asbeck et al., 2006b). The suspension system also works to passively distribute the overall load across an array of microspines (Kim and Cutkosky, 2008). These features allowed robots like RiSE (Spenko et al., 2006, 2008) and Spinybot (Kim et al., 2005) to climb flat, rough, vertical surfaces such as exterior brick and stucco walls.

To be useful for mobility on natural rock surfaces in space, this technology has been extended in three critical ways:

1. *New configurations of opposing microspines are used that can resist forces in any direction,*
2. *hierarchical compliance is employed to comply with the large-scale roughness and variation of rock surfaces, and*
3. *materials and mechanisms that can withstand the extreme environment of space are utilized.*

Hand-actuated conceptual prototypes of microspine grippers that pursued these technology goals were presented in Parness et al. (2012a). This paper describes more mature robotic grippers that have been integrated into the LEMUR IIB system. Quantitative testing of the new grippers on a variety of rock types shows the omnidirectional nature of each gripper, and the ability to repeatably and releasably anchor to many natural rock surfaces. With four grippers, the LEMUR IIB system was fielded in a variety of gravitational orientations, and mobility experiments were performed on two types of rock, namely vesicular basalt and a'a, that are representative of the rock types near lava flows and caves on Mars. Single gripper tests were performed on a much larger suite of rocks and other substrates to characterize the performance of the grippers on many potentially relevant surfaces for both Mars and asteroids. In parallel, a gripper was also integrated and tested with a rotary-percussive coring drill that can be used to acquire samples for *in situ* investigation or to be cached and returned to Earth. In sum, these activities constitute a proof-of-concept system for several future mission scenarios that were previously not possible.

Unlike other proposed extreme terrain rovers, LEMUR IIB does not require a tether. Previous work by several groups has demonstrated the validity of rappelling robots for situations in which an anchor can be created at the top of a crater wall or cliff face (Bares and Wettergreen, 1999; Bartlett et al., 2008; Huntsberger et al., 2007; Nesnas et al., 2008). The robot described in this paper can climb a cliff face from the top or bottom, and move laterally on the surface and across overhanging or steep slope sections equally well. In fact, LEMUR IIB even has the ability to climb on the ceilings of caves. The other major distinction is that with a self-anchoring robot like LEMUR IIB, which is similar to the architecture proposed in Yoshida et al. (2002) and Yoshida et al. (2003), mobility can also be achieved without a significant gravity field, as on the surface of a near-Earth asteroid. Rappelling robots are limited to bodies where there is a

significant gravitational field. The microspine grippers provide a true go-anywhere capability for consolidated rock surfaces.

2. MISSION SCENARIOS

The LEMUR IIB system could be used wherever consolidated rock is found in the solar system. Obvious applications are on the crater walls of Mars or the Moon, or on microgravity bodies like near-Earth asteroids. The system could also be deployed on Earth to conduct scientific investigations of canyons, cliffs, or caves, or in urban situations on the sides of buildings or across rubble piles created by disasters. Each of the potential NASA mission scenarios is described in more detail here.

2.1. Mars

Previous Mars rover missions have been limited by the mobility of the robot. Opportunity, the Mars Exploration Rover (MER), viewed stratified bedrock in the crater wall at Victoria Crater, but it was unable to approach and access the site despite the efforts of the rover drivers (Arvidson et al., 2006; Squyres et al., 2009). The six-wheeled rocker bogie architecture can overcome large obstacles, but limits rovers to slopes of $\sim 25^{\circ}$. For accessing crater walls, rappelling robots offer an attractive approach in certain scenarios in which the crater can be approached from above and a secure anchor can be positioned to support the descending robot (Bares and Wettergreen, 1999; Bartlett et al., 2008; Huntsberger et al., 2007; Nesnas et al., 2008), but they are more limited (as discussed in the Introduction) than a free-climbing system.

The surface of Mars is cold, dry, and subjected to heavy doses of radiation, making it an unlikely environment for current life. However, as noted in the Planetary Decadal Survey (Squyres, 2011), "*Mars's subsurface appears to be more hospitable.*" The recent evidence of liquid brines that may have subsurface sources makes the search for life underground even more compelling (McEwen et al., 2011). Mounting evidence of an extensive and highly biodiverse subsurface microbial biosphere on Earth existing on a variety of inorganic energy sources lends further plausibility to the idea (Boston et al., 2001). A free-climbing rover could access some of these subsurface locations on Mars, including the vertical entrance skylights to lava tubes, which have been observed by the Mars Reconnaissance Orbiter (Cushing et al., 2007; Cushing and Titus, 2010; Leveille and Datta, 2010). Caves can protect against thermal changes, wind, high intensity ultraviolet, and the extreme ionizing radiation environment. On Earth, it is no accident that some of our most exquisitely preserved paleontological remains, such as intact mummified thylacines, archaeological finds such as extractable Neanderthal DNA, and the earliest known textiles have all been found in caves. The LEMUR IIB system has the flexibility to access and acquire samples in these subsurface caves that no other robot could reach (Parness et al., 2012).

2.2. Human Exploration of a Near-Earth Asteroid

Near-Earth asteroids are a commonly discussed destination for human exploration (Obama, 2010). These asteroids do not have significant gravity wells, which reduces the mass of propellant required. However, this same lack of gravity necessitates more advanced technology for maneuvering on and interacting with the target. Few, if any, of the Apollo equipment development and surface operation lessons will be applicable.

The LEMUR IIB system presented in this paper could be used for a robotic precursor mission to obtain critical information about the target, such as toxicity, surface strength, and mineralogy, and could validate several capabilities such as surface anchoring and worksite stabilization, which were identified as "Strategic Knowledge Gaps" by NASA planning activities. If sent several months or more in advance of astronauts, the robot could also prepare the surface of an asteroid for astronaut exploration by using its drill to lay down an anchored network of cables, increasing the safety of the astronauts, and allowing more exploration and science to be done during the crew's limited time at the target. The system could also be teleoperated by astronauts or used autonomously to assist humans at the target.

2.3. Science Directorate Missions to Asteroids and Comets

The primitive material that asteroids and comets contain may date back to planetary accretion (Kleine et al., 2009; Zinner, 2003). Sampling and analyzing the rock and regolith on these bodies has the potential to answer longstanding questions about the formation of the solar system. Comets, in particular, also contain organic material that was identified in Wild 2 samples and through remote sensing observations (Kissel and Krueger, 1987; Sandford et al., 2006). The Astrobiology Roadmap prioritizes the exploration of cometary material because this organic content may be related to the origins of life on Earth (Des-Marais et al., 2008).

While small bodies can vary widely, the portfolio of objects that have been visited by spacecraft is growing and shows several commonalities. JAXA, ESA, NASA, and Roscosmos have all flown or have plans to fly to comets and/or asteroids. Unilaterally on every object that has been visited, large consolidated rocks have been observed. Examples of these can be seen in Figure 2. [Pictures of asteroid Itokawa were excerpted from Saito et al. (2006) and those of asteroid Eros were from Veverka et al. (2001).] Rock cores from these sites can provide scientific information that cannot be obtained from regolith samples or small rock fragments, including contextual information as well as geological features such as grain boundaries. Regolith samples

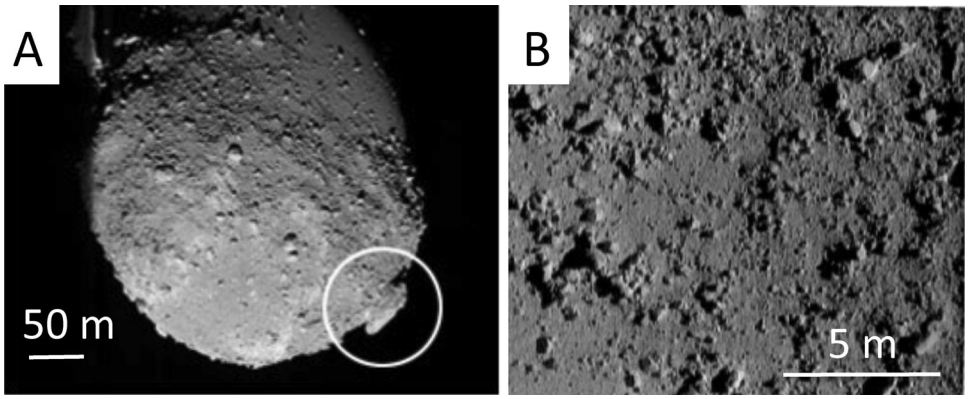

Figure 2. Large rocks can be seen in these close up images of asteroids (A) Itokawa and (B) Eros. The rock circled in (A) is approximately 50 m across. Core samples from these kinds of rocks have a high scientific value, and the rocks themselves have operational value as anchor points. Pictures of Itokawa reproduced from Saito et al. (2006) and those of Eros from Veverka et al. (2001).

from the surface will also be skewed to minerals that can survive the radiation exposure and may lack soft minerals that weather faster and may only be present beneath the weathering rind of a rock. Large rocks also provide an operational asset to missions. These rocks likely offer the most secure anchor points on the bodies, even (especially) for so-called rubble-pile asteroids. However, existing microgravity sample acquisition capabilities are limited to "Touch-and-go" techniques. The LEMUR IIB system demonstrates a way to remain on the surface for long periods of time. In some mission scenarios, expansion bolts could be placed in the bore hole after a sample has been acquired to provide a permanent anchor point.

2.4. Planetary Defense

Asteroids and comets are also important to the global community because of the threat of a collision with Earth that might cause extensive damage and loss of life, and in the worst scenario, could trigger human extinction. The recent IAA Planetary Defense Conference identified 350 near-Earth objects with a small but nonzero probability of impact this century (Ailor, 2011). NASA was ordered by the US Congress to create a catalogue of these potentially hazardous objects. While that survey is nearing its goal of 90% completion, technologies to alter the trajectory of an object are still immature (Shapiro et al., 2010). There are many proposed concepts, several of which would benefit from the LEMUR IIB system's capabilities, such as sustained mobility on the surface for placing reflectors or thrusters at prioritized locations, or the ability to drill into the subsurface of the object to place explosive charges. One thing that the entire community agrees upon is that knowing more about these objects will improve deflection strategies.

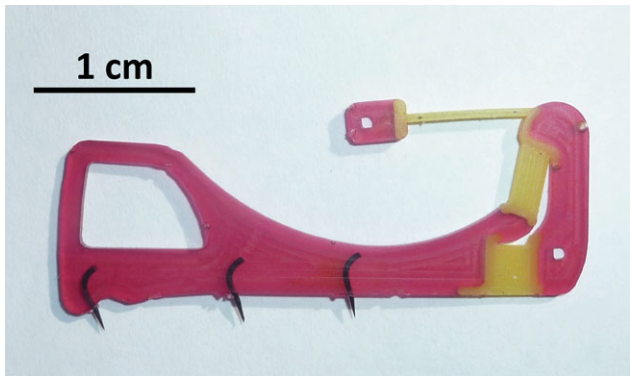

Figure 3. Microspines consist of a rigid frame (red), embedded steel hook, and elastic flexures (yellow) that allow the spine to both translate and rotate relative to its neighbors in order to find a suitable asperity on the rock to grip.

3. MICROSPINE GRIPPER DESIGN

Microspines were originally developed for vertical climbing robots (Asbeck et al., 2006a, 2006b). Similar biomimetic structures were also developed in Matthew et al. (2010). A single microspine, pictured in Figure 3, can be fabricated in a batch of 50–100 using the shape deposition manufacturing process (SDM). SDM uses sequential milling and casting steps to create multimaterial parts with embedded components (Merz et al., 1994). Each microspine is comprised of three elements: a rigid frame, compliant flexures, and one or more embedded steel hooks. Of these, the compliant flexures are the most important to a design. These flexures, whether made from elastomers or metal springs, allow each hook to move relative to its neighbors on its own suspension system. This way, when an array of microspines is dragged along a surface, individual hooks can grasp asperities in

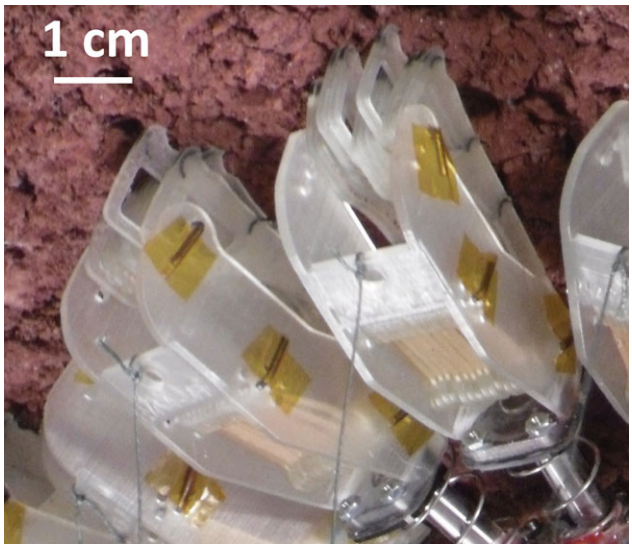

Figure 4. Close-up view of several carriages of microspines. The independent motion of both the microspines and the carriages relative to their neighbors can be seen. The ability to passively conform to variations at multiple length scales on the rock is key to achieving a successful anchor.

the rock at various points as they encounter good holding locations and share a small portion of the overall load. This independent stretching and force balancing can be seen in Figure 4, where neighboring microspines have found various pits and bumps on the rock to grasp.

To adapt the technology to rock-climbing for space applications, JPL's grippers use a radial arrangement of microspines with a centrally tensioning degree of freedom to create an omnidirectional anchor point. To conform to rocks, the gripper's hierarchical compliance system aligns to cm-scale features with 16 carriages, each of which contains 16 microspines that conform to mm-scale features and below. A torsion spring biases each carriage into the rock face regardless of gravitational orientation so that the microspines will drag across the rock surface and establish a grip, even in an inverted configuration.

Figure 5 diagrams many of the important components of the gripper explained here, and an assembled gripper can be seen in Figure 6. Moving beyond previous hand-actuated grippers, each gripper now uses two actuators for robotic operation. The *disengage actuator* pulls all of the carriages up and away from the rock surface. This actuator actually consists of three parallel linear actuators mounted around the outside of the gripper housing. By

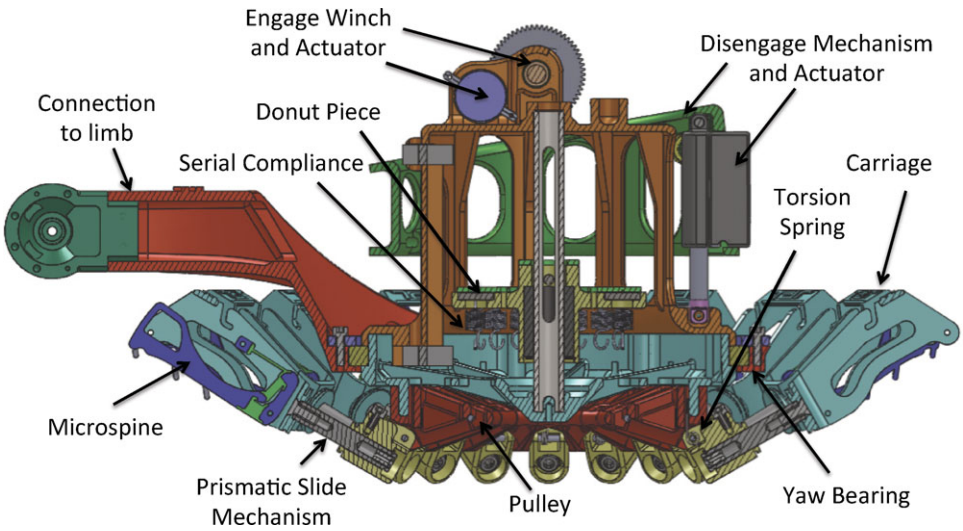

Figure 5. CAD representation of the microspine gripper with two active mechanisms and many passive degrees of freedom. The engage actuator powers a winch mechanism that raises and lowers the donut piece. Within the donut are 16 serial compliance elements that allow each carriage to move independently. These serial compliant elements (springs) are connected to the prismatic sliding mechanisms via cables (not shown) that wrap around fast pulleys. By raising the donut, the carriages of microspines are dragged along the surface of the rock, gripping the surface roughness in a squeezing motion. The disengage mechanism uses three parallel prismatic actuators (only one shown) to raise a ring that rides on the outside of the main gripper housing. This ring is connected via cables (not shown) to the base of each carriage, causing the carriages to rotate up and away from the rock when commanded. This actuator mechanism is strong enough to overcome the torsion springs that bias each carriage into the rock surface when the disengage mechanism is in the down position. A yaw bearing allows the limb to rotate with respect to an gripper so that twisting moments are not applied to the gripper during climbing.

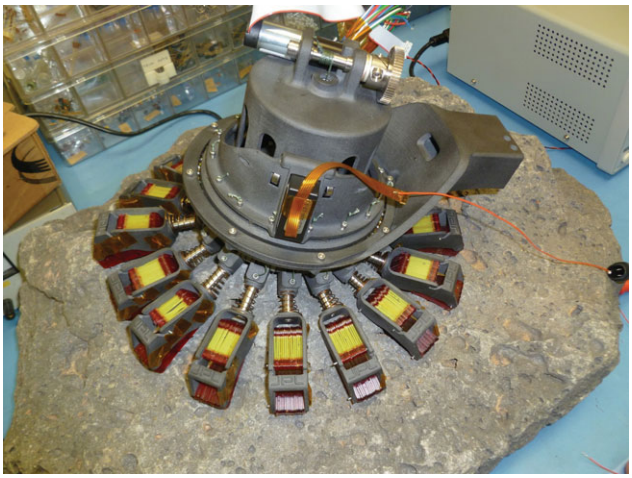

Figure 6. An assembled microspine gripper.

commanding these actuators to the up position, an outer disengage mechanism moves up relative to the central housing. Each carriage is attached to this ring by a thin disengagement cable, connected a short distance away from the mounting position about which the carriages pivot. The disengage actuation must overcome the bias of the torsion springs located within each carriage that pivot the carriages into the surface. By holding the carriages in the disengaged position, the chances of accidentally catching a microspine on the rock surface during movement of the leg is minimized. The new robotic grippers have a mass of 1.05 kg each.

When the gripper is ready to be engaged, the disengage actuator is commanded to the down position, the disengage mechanism lowers, and the torsion springs located within each carriage pivot the microspines into the surface of the rock regardless of the gripper orientation with respect to gravity. The second step in creating a secure anchor is to power the *engage actuator*. The engage actuator is a DC motor located on the top of the gripper housing. This motor is highly geared through a five-stage planetary gearbox, the output of which turns a winch mechanism. The winch raises a center donut piece that is connected to all of the carriages through another set of cables (engagement cables) with a series elastic spring element located at the donut interface. By winching up this center donut, all of the carriages pull inward in a prismatic manner. Each carriage is mounted on a dowel pin that is free to slide within a sleeve bearing, providing the prismatic motion. By applying tension to the engagement cables, the microspines are dragged along the surface of the rock giving them opportunities to catch on asperities. When a microspine catches, it bears load and the series elastic element connected to the donut extends instead of the carriage continuing to move inward. The donut is raised a fixed amount such that all of the carriages have had sufficient drag along the rock surface to allow the microspines to catch. If no microspines engage the surface, a carriage runs into a hard stop, and the donut spring extends a slight amount.

Tension in the engagement cables also creates a moment about each pivot point where the carriages are connected to the central housing, further pushing the microspines into the rock surface during engagement. The torsion spring is also mounted at this pivot point, so the carriage is naturally biased into the rock surface with a modest force enabling the spines to contact the surface before tension has been applied to the central gripping mechanism. This is the case even in zero gravity or inverted configurations. By varying the length of the dowel pin and the angle at which the cable pulls on the carriage, the magnitude of force being applied to each of the two motions (prismatic and rotational) can be traded against one another as shown in Figure 7. The relationship is described by

$$\sum M_{+} = M_k + T d_3 - R_x d_2 - R_y d_1, \tag{1}$$

where T is the tension in the cable, M_k is the moment created by the torsion spring, R_x and R_y are the reaction forces of the rock acting on the hook, and d_1, d_2, and d_3 are the lengths of relevant moment arms. This relationship becomes important to transducing the force that each carriage is supporting, as detailed below in the section on sensing. A conical spring returns the carriage to the fully extended state between each gripping sequence when the central tensioning mechanism is not applying any force.

To release the gripper, the process is reversed. The winch powered by the engage actuator is lowered, releasing the tension on all of the carriages and microspines. When all tension has been relieved, the disengage actuator is commanded to the up position and the carriages rotate up and away from the surface. In rare cases (less than 5%), a microspine does not release from the surface easily because it has become lodged in an asperity like a pit. In these cases, the robot's limbs can be used to dislodge the spines. Overload protection built into each microspine prevents the flexures from tearing, and instead causes a local rotation at the spine tip, aiding disengagement. In very rare cases (less than 1%), the spine still does not disengage. In these cases, the limb can be used to break the spine as a single microspine is weak compared to the limb actuators. While undesirable, each gripper has 256 microspines, so the loss of single spines at a slow rate does not impact overall mobility performance.

SDM and rapid prototyping processes such as selective laser sintering make rapid iteration of microspine and carriage designs possible, but the resulting polymer parts are not compatible with the space environment. An analog design that uses flight-qualified materials was constructed using the principles of microspine attachment (independent conformation, load sharing, opportunistic attachment via drag over a rough surface), but using metal spring

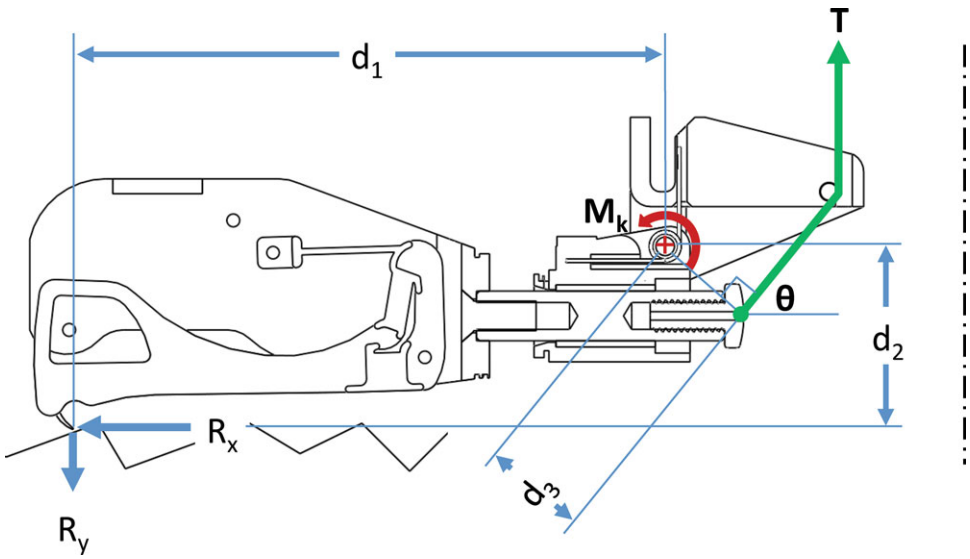

Figure 7. Free body diagram of the carriage subsystem assuming a fixed outer housing. The angle, θ, that the cable is pulled and the length of the dowel pin can be designed to influence the reaction forces at the hook tip.

Figure 8. A tension sensor was used to measure the anchoring strength of the flightlike gripper at various angles away from the rock surface. The gripper is shown here supporting >130 N normal, >150 N at 45°, and >140 N tangent to the surface of the rock. Scale readings are in lbf.

elements and containerizing the mechanism within a central housing. This implementation does not use any elastomeric polymers that are unsuitable for the very cold temperatures of space; it can be made entirely of metal. The design also shields the compliant mechanisms from debris and secures moving parts within a protected shell. However, this design had only 80 potential attachment points and a single level of compliance. The polymer version of the gripper achieved two levels of compliance, and 256 potential attachment points. Still, because of additional strength, 75% of the performance of the polymer gripper was realized with this flightlike design. Figure 8 shows the flightlike gripper supporting more than 130 N during pull tests tangent to the rock, at 45°, and directly away from the rock. Future grippers will try to capture the strengths of both of these approaches, as well as integrating the sensors discussed below.

4. CLIMBING ROBOT KINEMATICS AND CONTROL

The LEMUR IIB robot was fielded for mobility experiments on natural rock at various angles. Experiments included vertical climbing, climbing overhangs, and walking inverted on ceilings. LEMUR IIB was the last in a series of small utility robots built in the early 2000s (Kennedy et al., 2001). The robots were designed with swappable end effectors so that various tools could be integrated into the feet of the robot and used for repair, construction, and inspection of structures in space. LEMUR IIA is a hexapod with an upright posture that has the ability to crawl on a manmade structure (for example a hypothetical large space telescope). LEMUR IIB was originally designed to climb walls using human rock-climbing tools and strategies, or using drills to create its own footholds with each step (Badescu et al., 2005; Bretl et al., 2006; Kennedy et al., 2006). Driven by the mechanics of climbing a vertical cliff face, LEMUR IIB uses a sprawled posture to minimize the moments caused by the center of mass being offset from the wall. This made it the better choice for our own climbing experiments.

LEMUR IIB uses a PC104 electronics stack with a 266 MHz processor and 128 MB of RAM. The stack also contains an ethernet board, camera boards, digital IO, analog input boards, hardware filters, analog outputs, and several custom motor driver boards capable of sourcing up to 3 A of continuous current per channel. Further details can be found in Kennedy et al. (2006b).

The software environment for the LEMUR robots is written in ANSI C for the VxWorks operating system. It is architected in three layers: device driver, device abstraction, and application, with the interface to the robot hardware provided by the device driver layer (Kennedy et al., 2006b). The operator, using the application layer, can script a set of open-loop moves for the robot, which can be performed with autonomous gravity compensation. The device abstraction layer performs collision avoidance and computes joint-level commands based on Cartesian inputs from the user. Alternatively, the user can also step through joint level commands in a teleoperation mode.

At this time, LEMUR IIB is kinematically limited to planar climbing experiments by the three degrees of freedom it has in each limb. A yaw joint located at the body and a second yaw joint at the elbow allow each limb to trace a workspace in the plane parallel to the wall on which the robot is climbing. A single pitch joint at the elbow moves the end-effector up and away from the wall. However, because the microspine grippers are not pointlike feet, like those previously implemented on the robot (Bretl et al., 2006), scuffing could occur as the approximately 20-cm-diameter footprint of the microspine gripper is lifted away from the surface. The disengage degree of freedom in the gripper overcomes this limitation by pulling each carriage up and away from the surface before the foot is pulled away. During experiments, this limited scuffing and provided a smooth surface (instead of the sharp microspine hooks) that would slide rather than grip the rock. However, failure would sometimes occur if the local roughness of the rock exceeded the planar kinematics of the robot by more than ∼8 cm.

Future plans include expanding the kinematics of each limb to five active degrees of freedom or more so that the full six-dimensional climbing capability can be validated using the microspine grippers. A limb design with five active degrees of freedom would take advantage of the radial symmetry of each gripper while still accommodating more complex climbing scenarios such as curved rocks, plane changes, and concavities.

5. MOBILITY EXPERIMENTS

Several mobility experiments were performed with the LEMUR IIB system on natural rock surfaces at various orientations with respect to gravity. Two test setups were utilized for these experiments, one for inverted trials (ceiling-walking) and another that could be configured at various angles from a steep slope (60°) to slightly overhanging (105°). Each apparatus used reconfigurable tiles of natural rock. To create these tiles, the surfaces of large boulders were sawed off and glued to wooden squares. Mounting hardware was fixed to the back of each wooden square, allowing the rocks to be secured to either test apparatus. This modular system reduced the weight of the rock being supported by the apparatus and enabled rapid reconfiguration of the test setup to accommodate different rock types or to introduce macroscale geometric changes such as large bulges, steps, and holes in a variety of locations with respect to the robot. Each tile can be mounted in four different orientations and at any of the locations on either test apparatus.

Three test cases were performed with the robot: *vertical*, *105°* (slightly overhanging), and *inverted*. Figures 9, 10, and 11 show each case. Vesicular basalt and a'a lava rock were used as substrates to represent volcanic flows and lava tubes on Mars. To extend testing times and facilitate easy modifications to the gait sequence, offboard power was used and the robot was controlled through its ethernet port from a laptop. The robot operated using a quadrupedal gait with three grippers always attached to the rock to maximize the stability of the system. Due to limited range of motion and to simplify the gait, no body shifting was used during or between leg steps to keep the center of mass in a particular location within the stability triangle of the three remaining points of contact, although it is believed that using this strategy could reduce the maximum forces seen at any particular gripper. The center of mass was, in fact, likely outside of this triangle during parts of the motion, but the omnidirectional performance of the grippers was able to counteract the resulting forces and moments at each foot. The typical gait sequence employed was front left foot, front

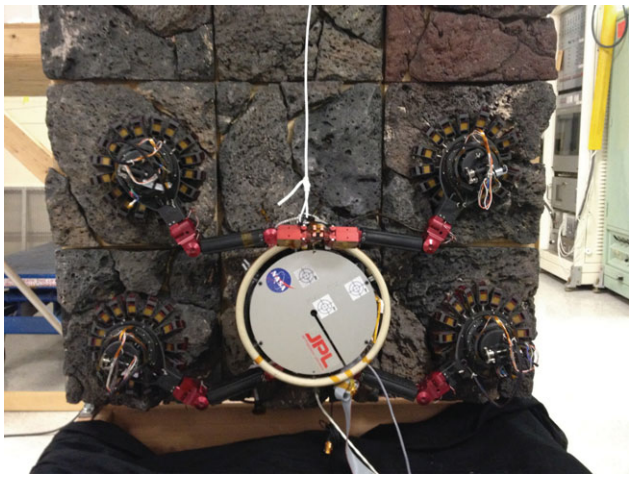

Figure 9. The LEMUR IIB system free-climbing up a vertical rock wall using microspine grippers.

Figure 11. The LEMUR IIB system climbing in a fully inverted configuration with a 30–60% gravity offload depending on position along the wall.

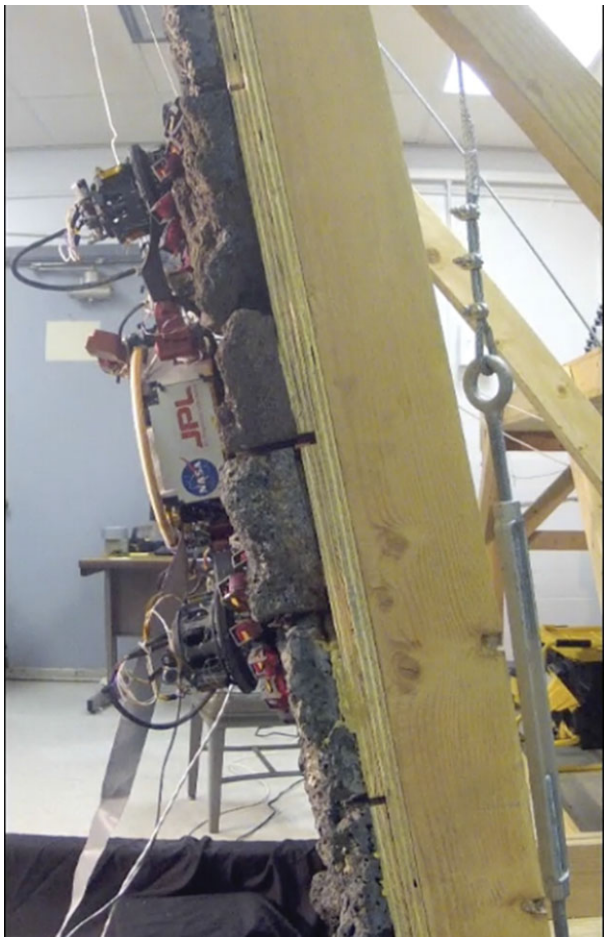

Figure 10. The LEMUR IIB system free-climbing up a 105° overhanging wall using microspine grippers.

right foot, back left foot, back right foot, and Cartesian body shift, as seen in Figure 12. Since each gripper could support the entire weight of the robot by itself, gripper failure was almost never the cause of climbing failure.

The robot successfully demonstrated mobility in each test case. However, in all three configurations, compliance within the grippers coupled with the limited degrees of freedom in each limb constrained the performance. In the case of vertical motion, the robot would sag slightly after each foot was released, resulting in a slower upward velocity than commanded. For the overhanging scenario, this same sag not only caused the robot to slip down the wall slightly with each step, but it also caused the center of mass to move slightly away from the wall, limiting the number of steps that could be taken before loss of contact with the wall. After approximately 15 steps at this angle, the microspine grippers could no longer engage the wall. This phenomenon occurred much more dramatically in the inverted case. As an inverted free-climber, the robot could only take three steps before the sag caused the next microspine gripper to be out of reach of the surface. This kinematic constraint was disappointing since each gripper could support the entire mass of the robot on its own. To compensate for the robot's limited kinematics in the inverted test case, a central gravity-offload cable was run down the center of the robot to relieve between 30 and 60% of the robot's weight depending on the robot's location on the ceiling.

Movies of each climbing trial can be viewed in Parness (2013) (youtube.com/watch?v=4JJfIEK0Adw).

6. SINGLE-GRIPPER EXPERIMENTS

To characterize the performance of the microspine grippers across a range of operating conditions, a single gripper was

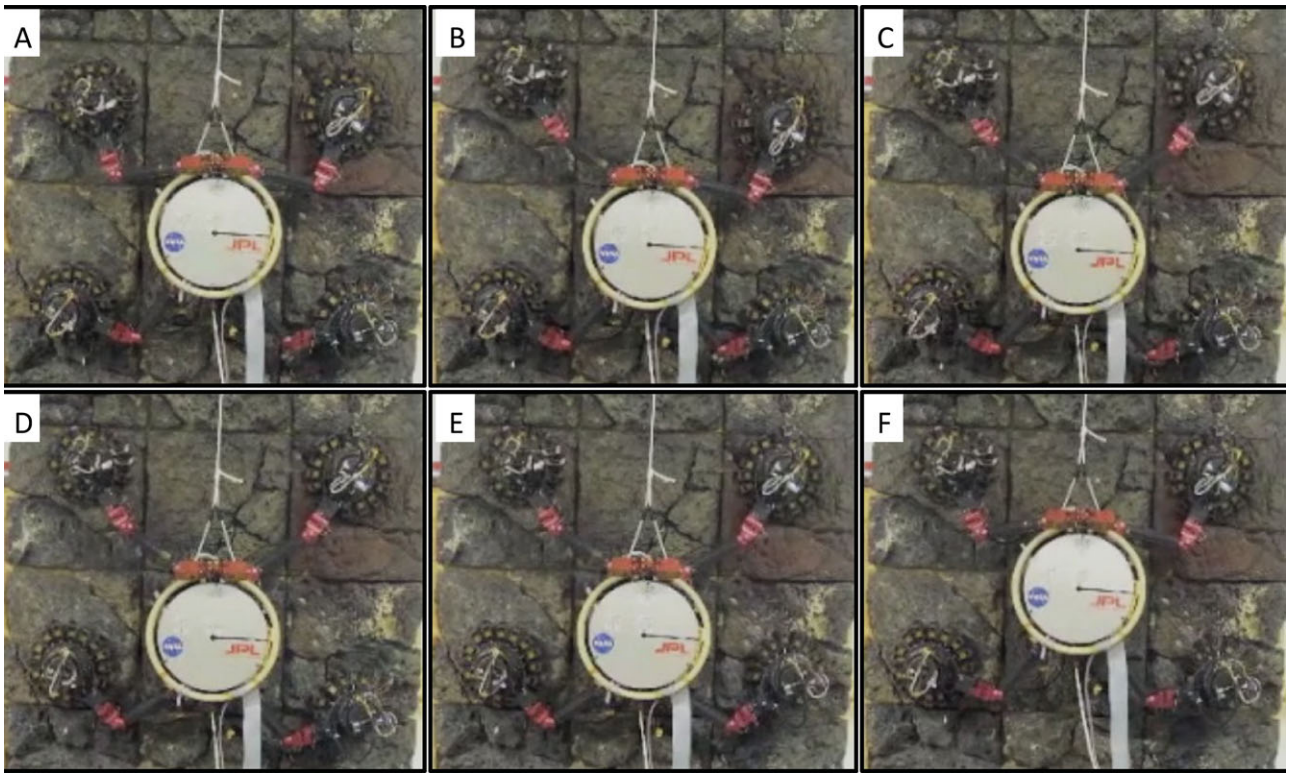

Figure 12. Sequence showing four steps and a body shift movement during a vertical free-climbing experiment using. Sag can be noticed as the body shifts down the frame with each step in pictures A–E before the body shift, despite the grippers moving up the wall. Improving the robot's kinematics and increasing its stride length could alleviate this phenomenon and allow the robot to take larger steps. In a lower gravity field (i.e., Mars or the Moon), this phenomenon would also be much less pronounced.

tested in an experimental rig on a variety of surfaces and at a range of pull-off angles. Materials were chosen to represent the possible surfaces that might be encountered on a near-Earth asteroid, and included both consolidated rocks and loose materials. It was expected that the grippers would perform poorly on the loose material. For the operational scenario of a microgravity body like an asteroid, it is likely that the robot would anchor, drill, and place permanent bolts in the large boulders, but walk slowly and without microspine gripping across the regolith that might separate these boulders. On some asteroids, the entire surface may be consolidated rock, or a large region that will be explored will be consolidated, for example the 50-m-diameter horn observed on the asteroid Itokawa.

The experimental apparatus consisted of a support cage, a digital force gauge with USB interface, a pulley system, and a horseshoe pivot. At the start of a test, the gripper is engaged to the test material using a teleoperation mode to run the motors. A cable is attached to the horseshoe pivot that interfaces to the gripper housing. This cable runs through several pulleys and a linear spring to a manual winch. The spring in series alters the effective stiffness of the cable so that the effective gear ratio of the winch is significantly reduced and more accurate readings can be taken. The digital force gauge (Cooper Instruments, M4-100) is also in series with this cable, and measures tension in the cable with better than 0.1 N accuracy at a sampling rate of 100 Hz. To acquire the pull-off force, the winch slowly increases the force applied to the cable until the gripper slips or is released from the surface. Data logging software from Cooper is used to measure the maximum force. The pulleys on the test bed can be positioned so that the force on the gripper is applied normal to, 45° to, and tangent to the material's surface, allowing the omnidirectional behavior of the system to be characterized. The horseshoe pivot system shown in Figure 13 was designed to apply the loads where the ankle meets the housing. This system pivots on ball bearings, allowing it to move in all directions with low friction. The pivot minimizes torques and moments on the gripper that would not be present in a climbing implementation where multiple grippers would be in contact with the surface.

Materials tested were bonded pumice, loose lava rocks (<5 cm diameter), pea gravel (<1 cm diameter), sand,

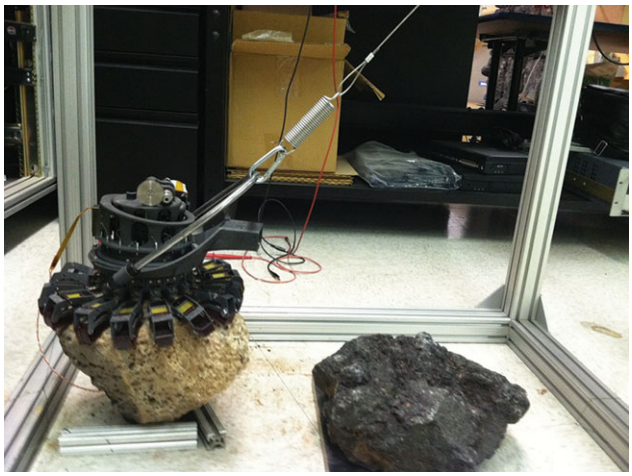

Figure 13. The single gripper experimental apparatus. The horseshoe piece pivots about the central housing, allowing various pull off force vectors to be applied to the gripper through the center of rotation, minimizing unwanted torques that would not be present in a climbing scenario with multiple feet in contact with the surface.

bishop tuff, saddleback basalt, vesicular basalt, and volcanic breccia. They are shown in Figure 14.

As expected, the gripper performed poorly in the loose materials, with virtually no distinction due to grain size or level of compaction, but showing some anchoring ability tangent to the surface in bonded granular material (designed to be similar to a comet surface). On the consolidated rocks, the gripper performed well for all rock types. The maximum holding capacity trended with the surface roughness of the rock sample, and in some cases was thresholded by the friability of the surface (i.e., the rock broke apart rather than the gripper slipping). Table I shows the average force (from five trials) at three separate pull-off angles (tangent, 45°, and normal). For bonded pumice and all of the unconsolidated materials (sand, loose lava rock, and pea pebbles), it was the material surface giving way that caused a failure rather than the release of the microspines.

Table I. Microspine gripper pull test.

Material	Normal (N)	45° (N)	Tangent (N)
Bonded pumice	2.2	1.0	45.4
Loose lava rock	2.7	0.3	0.5
Pea pebbles	3.1	1.1	0.4
Sand	0.3	0.2	0.7
Saddleback basalt	32.3	54.5	44.1
Bishop tuff	120.5	91.8	110.7
Vesicular basalt	189.5	113.2	281.4
Volcanic breccia	132.6	83.2	164.1

7. SENSOR INTEGRATION AND TESTING

The system can be improved by integrating sensors into LEMUR IIB's grippers to facilitate the development and implementation of closed-loop control policies that would enable robust climbing of surfaces with a variety of properties and topographies. Examples of control strategies that could be implemented on the robot include controlling the center of mass of the robot in order to optimally distribute loads among grippers, taking advantage of kinematic redundancy in the limbs in order to apply microspine engagement forces using the robot's limb actuators in addition to the normal engagement actuators, and retrying gripping if grip is lost

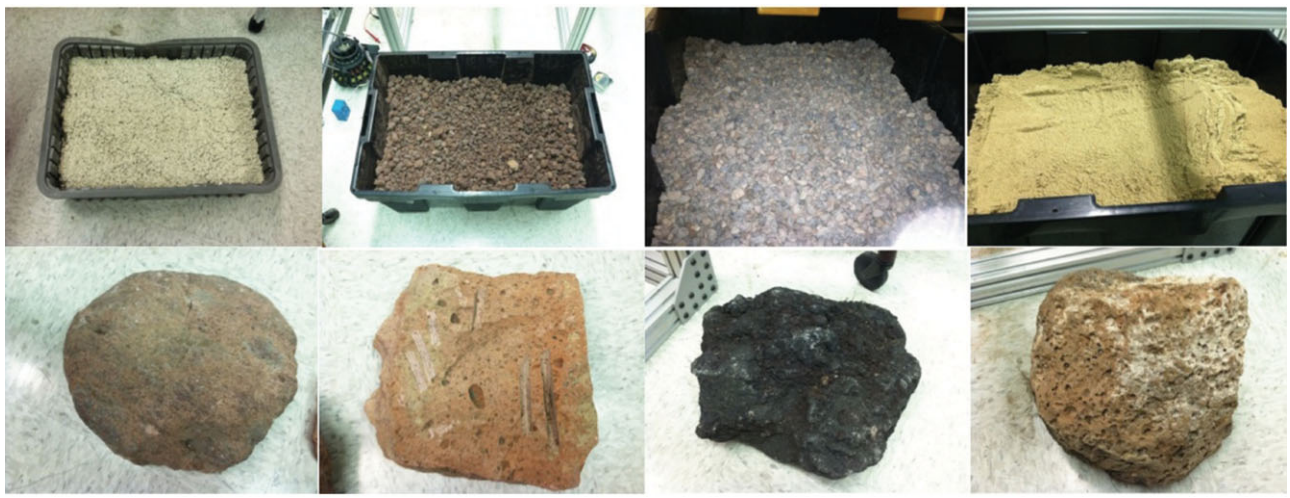

Figure 14. Test materials (top left to bottom right): Bonded pumice, loose lava rock, pea pebbles, sand, saddleback basalt, bishop tuff, vesicular basalt, and volcanic breccia.

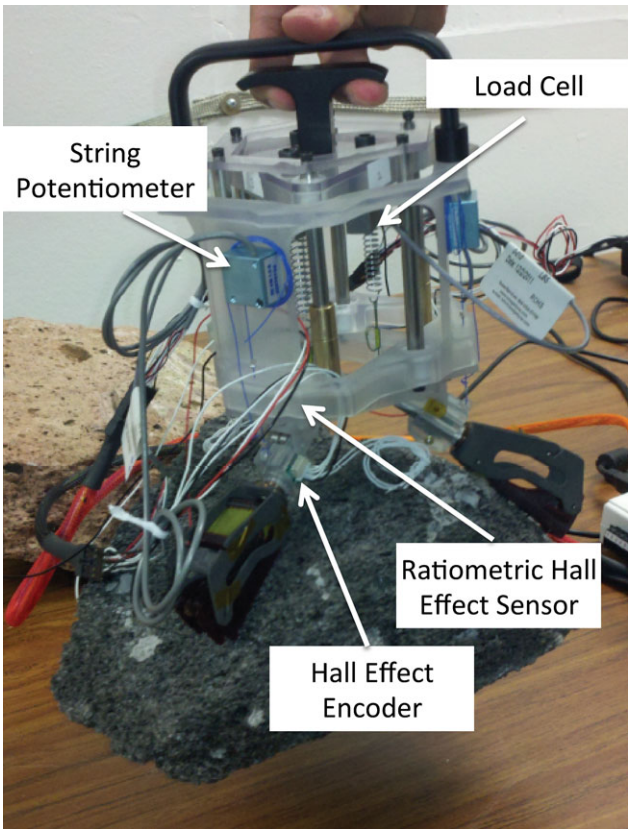

Figure 15. Hand actuated sensor test gripper with three carriages. String potentiometers, ratiometric Hall effect sensors, load cells, and linear Hall effect encoders were integrated into each carriage to prototype different potential sensing modalities.

or cannot be established on the rock surface in a specific location. To facilitate the implementation of these algorithms, information about the quality of grip must be transduced.

To evaluate and test various force sensors, a smaller test-gripper, seen in Figure 15, was designed and outfitted with several competing sensing solutions. The carriages, like in LEMUR's grippers, possess two primary degrees of freedom: a revolute joint and a prismatic joint. To sense the force vector acting on each carriage, two sensors are required. Several sensor combinations were prototyped on the test-gripper. All of the combinations involve one device for measuring the angular position of a carriage and one type of linear measurement device for the prismatic joint. Using the angular and linear position data for each carriage obtained by these sensors, the forces in the engagement cables can be obtained by calculating the extension of the springs in series with the engagement cables. To do this, an analytic kinematic model of the gripper was developed that allows one to obtain a relationship between the angular and linear position of the microspine carriages and the force experienced by those carriages.

String potentiometers mounted on the outer housing were considered for the angular position sensor. The string potentiometer cables served two purposes, working as both the disengagement cables and as part of the sensor. As a carriage moved through its angular range, the cable extended and changed the output voltage at the base. A second angular position sensor evaluated was a ratiometric Hall effect sensor. These devices were mounted on each carriage and paired with a permanent magnet attached to the underside of the central housing. As a carriage moved through its angular range, the distance between its Hall effect sensor and the permanent magnet changed, causing a change in output voltage.

As a linear sensor, load cells were placed in series with the engagement cables and springs and could directly measure the magnitude of force on each carriage, serving as a ground truth for other sensors. As a second option, linear Hall effect encoders were mounted on the carriage slide housings using simple custom circuit boards to measure the displacements of the carriages relative to the central housing. The sensors measured the displacement of a small magnetic strip embedded in each carriage's dowel pin, which has alternating north and south poles at 2.4 mm increments. As these poles moved under the chip, they generated a sine wave of voltage across the chip's five Hall effect sensors, which was encoded into a quadrature output in order to capture both the distance and the direction traveled.

Other sensors considered for measuring the spring extension included linear potentiometers, linear variable differential transformers, and optical sensors from computer mice. These solutions were not prototyped due to space constraints within the inner housing where the extension springs are located. Also considered was the use of buttons or limit switches that would trigger when a carriage fully traversed its linear range. These kinds of sensors would only provide binary "gripped" or "not gripped" data, as a loaded carriage generally will not fully retract. Lastly, computer vision approaches were also considered but were not pursued due to the occlusion of carriages by the central housing and connection to the robot limb.

Two National Instruments data acquisition systems were used to interface all the sensors with a laptop computer during experiments. A MATLAB program filtered and processed these data and then calculated the forces on each carriage separately based on the string potentiometer and the linear encoder pair, and the Hall effect sensor and the linear encoder data pair. Data from the load cell were also logged for subsequent ground truth comparisons. The forces on the gripper as well as errors between the calculated forces and the forces read from the load cell could then be plotted in real time and saved to a disk.

The first experiment recorded and compared the forces measured by the load cell with the calculated forces from

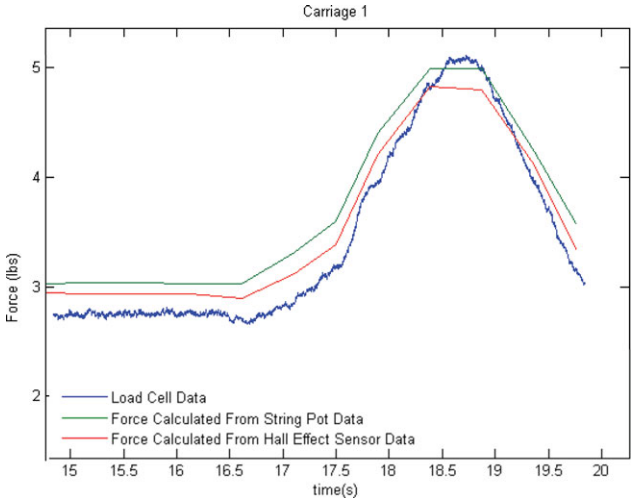

Figure 16. Data from the three sensing solutions during the gripping event: load cell ground truth, string pot system, and Hall effect sensor pair. Data taken from carriage number 1, but they are typical of all carriages and all trials.

each pair of sensors [(1) the linear encoder and string potentiometer combination, and (2) the linear encoder and Hall effect sensor combination] as a carriage was displaced through its angular and linear ranges. Figure 16 shows these forces along with the errors between the ground truth load cell data and each of the sensor combinations. These results show that the force measured by the load cell and the force calculated from the position sensor data correspond strongly. Additionally, the permanent magnet used by the ratiometric Hall effect sensor did not hinder the operation of the linear Hall effect encoder.

During angular range tests, the forces were as expected based on the analytic model. Errors in the sensor output decreased for both sets of sensors as the angle was increased. Similar results were obtained during the linear range test as the measured and calculated forces follow each other very well and correspond closely to the forces. Errors in the sensed value were small (<5%) and remained roughly constant throughout the linear range, except for a momentary increase in error when the carriage was first loaded.

The gripper was also subjected to a second set of experiments with various applied loads. When engaged on a rock and subjected to 0, 14, and 23 N loads, the measured and calculated forces from all three carriages were recorded and compared. No statistically significant drift was observed in the sensor position readings under various loads on the rock. The load experienced by individual carriages is not strongly correlated with the external load placed on the gripper.

Both sets of sensors provided similar results and errors in each set of experiments. However, the combination of the ratiometric Hall effect sensor and the linear encoder has many advantages over the string potentiometer and/or the load cell. First, ratiometric Hall effect sensors are very inexpensive and can be obtained for less than $2 each, whereas the string potentiometer costs $245 and a small load cell that can fit in the LEMUR IIB's gripper costs $750 (USD). Moreover, the ratiometric Hall effect sensors are the simplest to integrate into LEMUR's existing microspine grippers as they only require modification of the carriages and not the central housing or engagement and disengagement devices.

Subsequent work will include implementing a force-sensing solution on all of LEMUR IIB's grippers in order to enable the robot to scale vertical and inverted rock surfaces using closed-loop control. These control algorithms will be much more robust and fault-tolerant than the open-loop sequences currently being used. Using the test gripper's MATLAB software, pertinent information can be gathered to aid the development of these algorithms.

8. SAMPLE ACQUISITION TOOL DESIGN AND EXPERIMENTS

A microspine gripper was integrated with a rotary percussive coring drill to produce a sample acquisition instrument that can obtain a subsurface core from consolidated rock without requiring any externally applied forces. The instrument is self-contained, redirecting the load path back into the rock, with the forces being reacted by the microspine gripper. It can be seen drilling into a piece of vesicular basalt in an inverted configuration in Figure 17, and in a horizontally gravity off-loaded configuration in Figure 18.

A simplified free-body diagram of the gripper and drill system is shown in Figure 19 to illustrate the relationship between the gripping carriages and the preload that is applied to the drill bit, also known as the weight-on-bit. The weight-on-bit is directly proportional to the strength of attachment between the microspines and the rock. And although it is not shown, the torque reacted by the drill bit is directly proportional to the strength of attachment between the microspines and the rock in the z direction (tangent to the circle).

$$R_{\text{drill}} = R_{y1} + R_{y2}, \tag{2}$$

$$R_{x1} = R_{x2}, \tag{3}$$

where R_{y1}, R_{y2}, R_{x1}, R_{x2}, and R_{drill} are the reaction forces of the rock acting on the microspine drill instrument.

Adding a sample acquisition tool to a microspine gripper requires that an unimpeded cylindrical channel down the center of the gripper for the drill bit to translate through is maintained. Therefore, a new mechanism that pulls the engagement cables was created using a custom-designed linear actuator. The linear actuator consists of a circular plate that houses the extension springs and cables. The plate is built with three ball screw nuts that ride on three ball screws (Heli-Tek Corp.). The ball screws are connected at their ends to spur gears via Fair-Loc Hubs and the gears are meshed

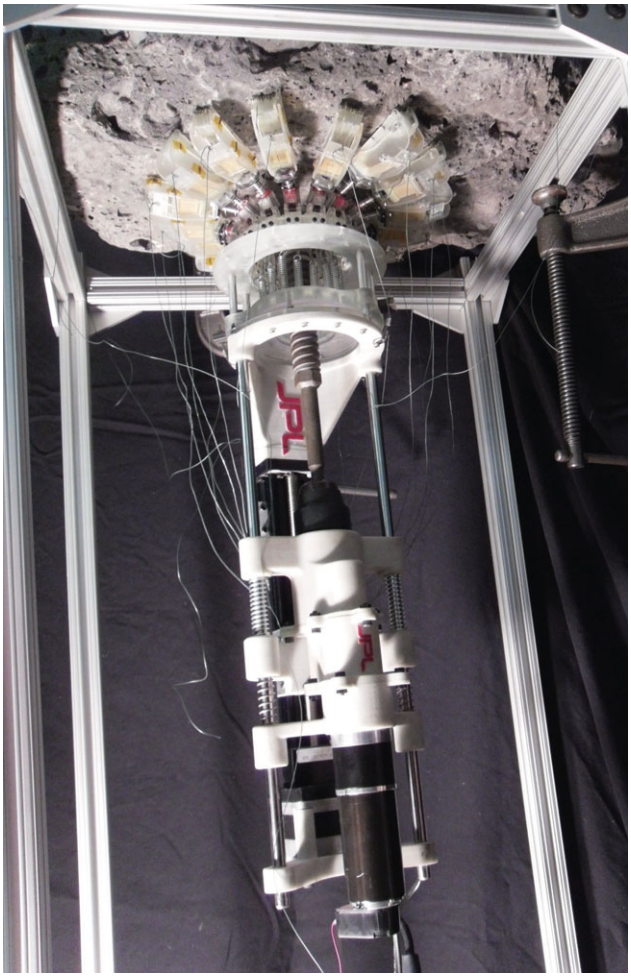

Figure 17. The Microspine drill coring into a piece of vesicular basalt in an inverted configuration on Earth. The instrument creates a 20-mm-diameter borehole up to 82 mm deep in the rock while retaining a 12-mm-diameter rock core sample.

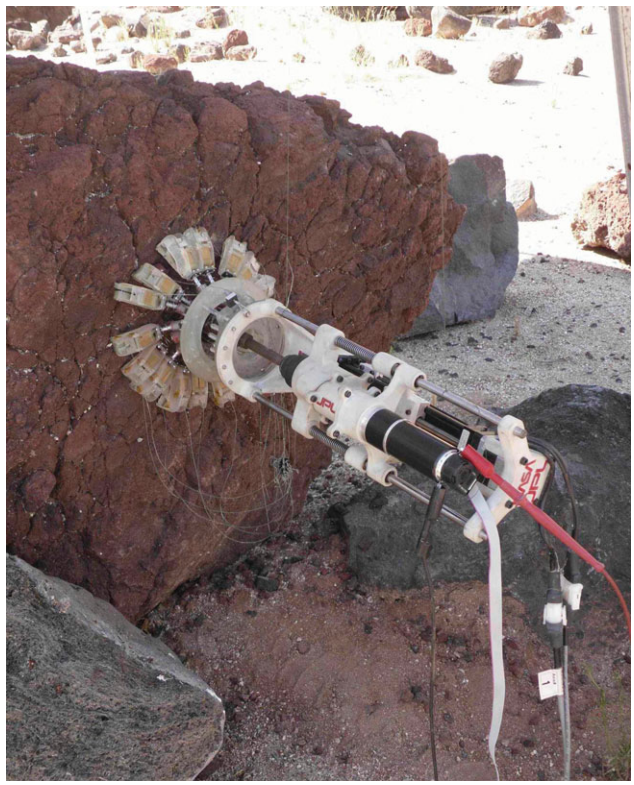

Figure 18. Horizontal drilling test with the microspine drill performed in a gravity offloaded configuration. A single microspine gripper can support forces in any direction, but is unable to support the moments created by the center of gravity of the system being offset from the rock while in a horizontal configuration. However, these moments can be reacted on a multilegged robot. Fishing line was used to react this moment during these tests while the microspine gripper reacted all the forces of drilling (i.e., weight-on-bit, vibrational loads, etc.).

in a planetary arrangement to a sun gear (SDP-SI) that rotates on the outside of the cylinder that the drill bit passes through. The planetary gear arrangement effectively creates a kinematic pair in which the rotation of the sun gear causes the linear displacement of the circular plate. The geometry of the ball screws on the circular plate causes them to self-react the torques they apply on the plate, forcing the plate to stay parallel to the plane orthogonal to the drilling axis. This mechanism also forces concentricity with the drilling axis during actuation. The sun gear is driven by another spur gear that is connected to a 12 V DC brushed motor (Maxon Motor USA). A CAD model of this arrangement is shown in Figure 20.

Ball screws were chosen over standard ACME threaded lead screws due to their low friction. Radial and thrust bearings were used throughout the mechanism to reduce friction. The total friction in the system was approximated as an efficiency, which was used to calculate the necessary torque to be delivered by the DC motor and to measure its planetary gear box. This relationship is described by the following:

$$T_m = (FL/2\pi)N_{\text{spur}}N_{\text{planetary}}1/e, \tag{4}$$

where T_m is the motor torque, F is the load on the ball screw due to tension, L is the pitch of the ball screws, N_{spur} is the number of teeth on the spur gears, $N_{\text{planetary}}$ is the planetary gear box ratio, and e is the efficiency of the system. The number of teeth on the sun gear is irrelevant because it acts as an idler.

A rotary percussive drill was chosen instead of a rotary drill for efficiency and speed on hard rock (Zacny et al., 2008), mimicking the decision to fly a rotary percussive

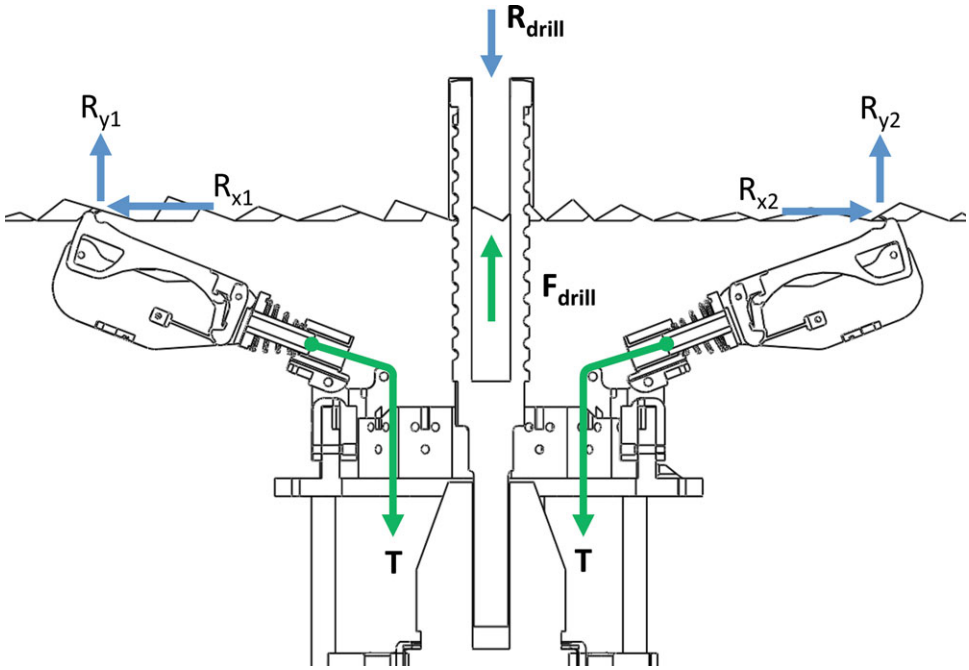

Figure 19. Two-dimensional free-body diagram of the microspine gripper and drill system. The reaction forces are shown in blue, and the internal forces are shown in green. Clearly, the maximum weight-on-bit is limited by the strength of the anchor.

drill on the Curiosity Mars Rover (Okon, 2010). A commercial Bosch rotary hammer drill was used based on its successful use in prototype development for a Mars Sample Return sample acquisition and caching subsystem (Backes et al., 2010; Younse et al., 2010). The similarity of design will allow future versions of the microspine drill to integrate seamlessly with the current state-of-the-art sample caching systems (Backes et al., 2011).

Linear translation of the drill was accomplished by mounting the drill subsystem on a linear stage driven by a 24 V stepper motor (Velmex Corporation X-Slide). Two guide rails held sets of preloaded compression springs that dampened the percussive loads transmitted by the drill. For power, three lithium-polymer batteries were used, mounted inside of a polycarbonate container on the side of the drill.

Two versions of the drill were fabricated. The first, shown in Figures 17 and 18, is currently teleoperated, but designed to be integrated with the LEMUR IIB robot. The second version of the drill, shown in Figure 21, is designed as a hand tool for an astronaut to be used at near-Earth asteroids where there is insufficient gravity to react the forces and torques of drilling. Two handles were mounted to the drill and large toggle switches were used to close loops to the various DC motors so that the drill could be operated by an astronaut wearing pressurized gloves, which significantly restrict dexterity. For the linear stage, switches controlled a stepper motor driver (Pololu Corp.) and a frequency input from an RC-555 timer circuit that drove the linear stage at 7 mm per second. After final assembly, the astronaut version of the system had a mass of 8.44 kg.

Simulating microgravity conditions on Earth is difficult. Current methods include testing in neutral buoyancy pools or onboard aircraft flying parabolic trajectories. However, these methods are costly and have additional constraints. For instance, testing in a neutral buoyancy pool requires the system to be hermetically sealed; testing in an airplane flying a parabolic trajectory limits the duration of the test to approximately 20 s. Rather than meet these constraints, three testing configurations (inverted, horizontal, and astronaut-like) were established that constituted *harder-than-zero-g* or *near-zero-g* loading conditions.

For each test configuration, the following sequence of operations was used:

1. Establish the anchor using the microspine gripper,
2. deploy the drill into the rock with ~60 N weight-on-bit,
3. begin drilling,
4. drive the drill into the rock using the linear slide,
5. retract the drill bit after the desired depth has been reached,
6. cease drilling, and
7. evaluate the retained core sample and shavings.

For inverted drill tests, such as those in Figure 17, a test stand built from aluminum extrusion suspended a piece of rock in the air, leaving the bottom face of the rock exposed.

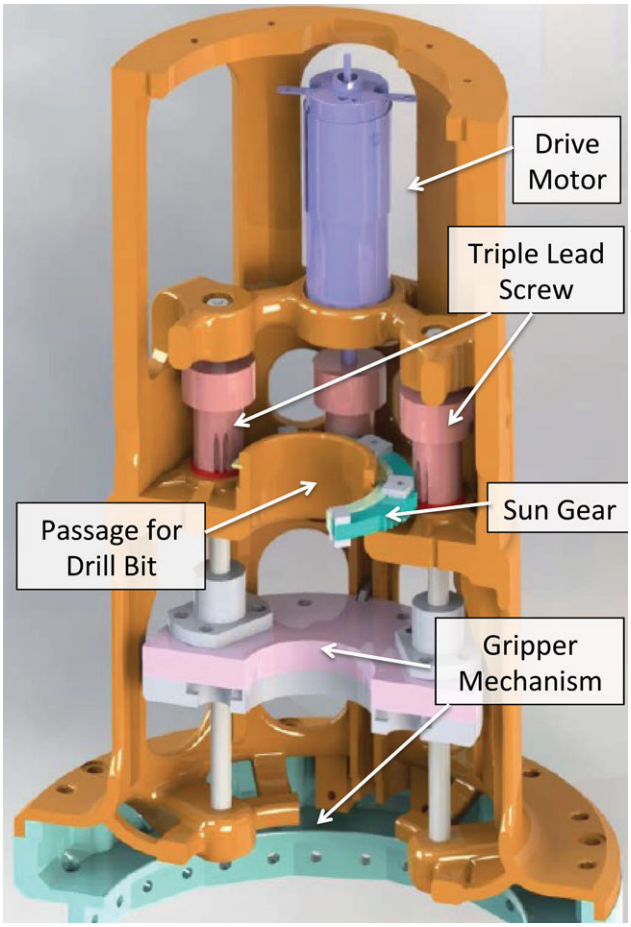

Figure 20. CAD model of the linear actuator for the gripper engagement: Orange represents the housing for the actuator, manufactured using stereo-lithography. Light pink represents the circular plate that houses the spring-cable elements. The ball screws and accompanying ball screw nuts are shown in gray, the nuts are mounted to the circular plate and the ball screws are constrained at either end of the housing, laterally by radial ball bearings and axially by retaining rings and a step on the screw output shaft. The ball screws are rotationally constrained to spur gears (dark pink), which transmit the thrust load into the housing on thrust ball bearings (red). The spur gears are meshed to a sun gear (teal), which is driven by another spur gear that interfaces with the DC motor and its planetary gearbox output (purple). The actuator had to be designed so that the motor could produce enough torque to apply the full tension load to the cables without stalling.

The teleoperated drill was used in this case, and the drilling sequence was performed. For horizontal drill tests, such as those seen in Figure 18, a large rock was chosen with a vertical face and the drill sequence was carried out. During these tests, a piece of fishing line was used to react the moment created by the center of mass of the drill being offset from the rock surface. Other drilling loads were reacted by the microspine gripper. To test the astronaut version of the drill, analog astronaut gloves were worn during testing to simulate the restricted dexterity astronauts have while wearing their gloves. The simulated gloves consisted of four layers: a latex glove, a wool glove, a thick rubber glove, and a leather work glove. For this test, rocks with masses ranging from 2.5–7 kg were lifted using the drill's microspine gripper, and then the drill sequence was carried out. Figure 21 shows this test configuration.

Figure 21. The handheld microspine drill is an instrument capable of anchoring to and coring into consolidated rock regardless of the magnitude or orientation of a gravitational field (1 g or less). The instrument is shown here coring into a piece of vesicular basalt while lifting that piece of rock.

The microspine-based drills successfully cored in all three test configurations on multiple rock types, including vesicular basalt and a'a lava rock. Bore speed was dependent on the weight-on-bit, drill speed, and material properties of the rock, but nominally ranged from 15 to 45 mm/min. A carbide-tipped coring bit created a 20-mm-diameter bore hole to depths ranging from 25 to 82 mm for the inverted drill test, and 15 mm for the horizontal drill tests and testing with the astronaut version of the drill. The retained core samples measured 12 mm in diameter and

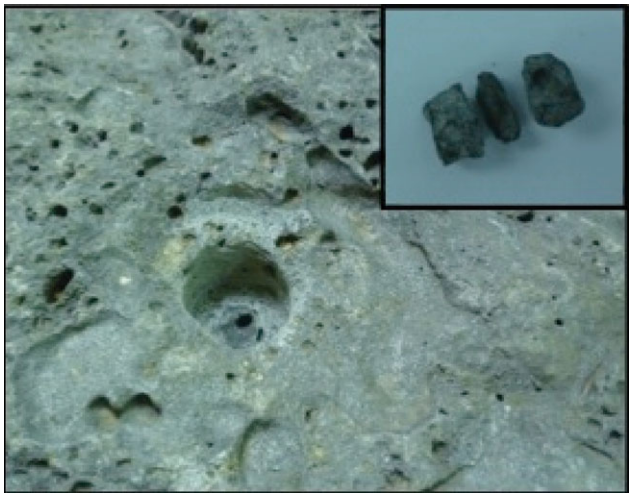

Figure 22. A borehole and retained rock core from an inverted drill test on vesicular basalt.

usually were extracted in several broken pieces, but with stratigraphy maintained. While a broken core may not always be desirable, it does eliminate the need to perform core breakoff. The residual bore holes and retained rock core can be seen in Figure 22.

During the drill process, failure most often occurred during hole-start. The bit would sometimes wander before achieving a good hole-start. Occasionally, this caused the microspine gripper to lose its grip. This was accentuated by the built-in compliance in the microspine gripper, which must resist the wander. However, this compliance also acts to dampen the vibrational forces, and is essential to the load sharing within the gripper.

Video footage of the drilling process can be seen in Parness (2013) (youtube.com/watch?v=4JJfIEK0Adw).

9. CONCLUSIONS AND FUTURE WORK

This paper presents mobility experiments for a 10 kg rock-climbing robot, LEMUR IIB, using microspine grippers. Vertical and overhanging (105°) free-climbing were demonstrated, and fully inverted mobility was demonstrated with a 30–60 % gravity offload. Single-gripper tests were also presented that characterized the grippers' performance on a variety of rock types similar to those that would be found on Mars or asteroids. A single gripper supported more than 100 N on a suite of consolidated rough rocks such as vesicular basalt, a'a lava rock, and volcanic breccia. The grippers were able to support these high loads in any direction away from the rock, including both normal and tangent to the rock.

An overview of the fielded system was described. Details were presented on the evolution of microspine grippers from hand-actuated prototypes that were previously presented (Parness et al., 2012b) to robotic grippers that are integrated with the robot system. Both the engage and disengage mechanisms through which 256 microspines are controlled through two actuators and the hierarchical compliance in the design that helps the microspines conform to roughness in the rock that exists at multiple length scales are explained. A more flightlike design that does not require the use of any plastic materials is also presented. The first prototype of this flightlike gripper achieved approximately 75% of the performance of the micrsopine grippers that were used on the LEMUR system. Small gripper prototypes that integrated sensors into carriages of microspines were also presented. The combination of two Hall effect sensors was shown to adequately measure the force on a single carriage, and could allow more autonomous and sophisticated control in the future.

This work constitutes a proof of concept for a new legged, self-anchoring rover architecture that has cross-cutting applications. Several mission scenarios that would benefit from the LEMUR system's capabilities were discussed, including the following:

1. Missions to extreme terrain on Mars,
2. manned missions to near Earth asteroids,
3. science missions that would utilize sustained surface operations on primitive bodies, and
4. planetary defense mission applications.

Acquiring rock cores with a rotary percussive drill that was integrated with a gripper was also demonstrated in three different experimental configurations. This suggests an operational paradigm that could both cache scientific samples and use the resulting boreholes to place permanent anchors with expansion bolts. These could be used to secure networks of ropes for astronauts exploring a microgravity surface or to provide additional safety to the rover as it maneuvers into a lava tube or across a microgravity surface.

Additional work is required to validate the full 6D climbing scenario. By adding additional active degrees of freedom to the limbs, not only will the system be able to climb across a fuller set of geometries including curves, plane changes, and large bulges or holes, but the largest limitation of the current system, sag from the compliance in the grippers, will be obviated. Future work will focus on adding degrees of freedom to the limbs and integrating hall-effect sensors that were prototyped on a 3-carriage gripper onto all 64 carriages on the robot. With these hardware upgrades, the team will be able to focus on closed-loop climbing algorithms and integrating inputs from LEMUR's stereo vision cameras that will allow a supervised autonomy style of control, like what would be required for flight operation.

ACKNOWLEDGMENTS

The research was carried out at the Jet Propulsion Laboratory, California Institute of Technology, under a contract with the National Aeronautics and Space Administration. Additional thanks to the JPL Office of the Chief Scientist and Chief Technologist and the NASA and JPL Education Offices.

MULTIMEDIA FILES

A 3-minute video is included as a multimedia attachment. This narrated video shows climbing trials and sample acquisition experiments.

REFERENCES

Ailor, W. (2011). Summary of the 2011 IAA planetary defense conference. 54th Session of the United Nations Committee on the Peaceful Uses of Outer Space.

Arvidson, R., Squyres, S., Anderson, R. et al. (2006). Overview of the Spirit Mars exploration rover mission to Gusev Crater: Landing site to Backstay Rock in the Columbia Hills. Journal of Geophysical Research, 111.

Asbeck, A., Kim, S., McClung, A., Parness, A., & Cutkosky, M. (2006a). Climbing walls with microspines. IEEE ICRA.

Asbeck, A., Kim, S., Provancher, W., Cutkosky, M., & Lanzetta, M. (2005). Scaling hard surfaces with microspine arrays. Robotics: Science and Systems. Cambridge, MA, USA.

Asbeck, A. T., Kim, S., Cutkosky, M. R., Provancher, W. R., & Lanzetta, M. (2006b). Scaling hard vertical surfaces with compliant microspine arrays. International Journal of Robotics Research, 25(12), 1165–1179.

Backes, P., Lindemann, R., Collins, C., & Younse, P. (2010). An integrated coring and caching concept. IEEE Aerospace.

Backes, P., Younse, P., DiCicco, M., Hudson, N., Collins, C., Allwood, A., Paolini, R., Male, C., Ma, J., Steele, A., & Conrad, P. (2011). Experimental results of rover-based coring. IEEE Aerospace.

Badescu, M., Bao, X., Bar-Cohen, Y., Chang, Y., Dabiri, B., Kennedy, B., & Sherrit, S. (2005). Adapting the ultrasonic sonic driller corer for walking climbing robotic applications. Proceedings of the SPIE, 5762, 160–168.

Bares, J., & Wettergreen, D. (1999). DANTE II: Technical description, results, and lessons learned. International Journal of Robotics Research, 18(7), 621–649.

Bartlett, P., Wettergreen, D., & Whittaker, W. (2008). Design of the SCARAB rover for mobility and drilling in the lunar cold traps. Proceedings of International Symposium on Artificial Intelligence, Robotics and Automation in Space.

Boston, P., Spilde, M., Northup, D., Melim, L. et al. (2001). Cave biosignatures suites: Microbes, minerals, and Mars. Astrobiology, 1, 25–55.

Bretl, T., Rock, S., Latombe, J., Kennedy, B., & Aghazarian, H. (2006). Free-climbing with a multi-use robot. Experimental Robotics IX, 21, 449–458.

Cushing, G., & Titus, T. (2010). Caves on Mars: Candidate sites for astrobiological exploration. Astrobiology Science Conference.

Cushing, G., Titus, T., Wynne, J., & Christensen, P. (2007). Themis observes possible cave skylights on Mars. Geophysical Research Letters, 34.

Des-Marais, D., Nuth, J. et al. (2008). The NASA astrobiology roadmap. Astrobiology, 8(4).

Desbiens, A. L., Asbeck, A., & Cutkosky, M. (2010). Hybrid aerial and scansorial robotics. IEEE ICRA.

Desbiens, A. L., Asbeck, A., & Cutkosky, M. (2011). Landing, perching and taking off from vertical surfaces. International Journal of Robotics Research, 30(3), 355–370.

Huntsberger, T., Stroupe, A., Aghazarian, H., Garrett, M., Younse, P., & Powell, M. (2007). TRESSA: Teamed robots for exploration and science on steep areas. Journal of Field Robotics, 24, 1015–1031.

Kennedy, B., Aghazarian, H., Cheng, Y., Garrett, M., Hickey, G., Huntsberger, T., Magnone, L., Mahoney, C., Meyer, A., & Knight, J. (2001). LEMUR: Legged excursion mechanical utility rover. Autonomous Robots, 11, 201–205.

Kennedy, B., Okon, A., Aghazarian, H., Badescu, M., Bao, X., Bar-Cohen, Y., Chang, Z., Dabiri, B. E., Garrett, M., Magnone, L. et al. (2006a). LEMUR IIB: A robotic system for steep terrain access. Industrial Robot: An International Journal, 33, 265–269.

Kennedy, B., Okon, A., Aghazarian, H., Garrett, M., Huntsberger, T., Magnone, L., Robinson, M., & Townsend, J. (2006b). The LEMUR II class robots for inspection and maintenance of orbital structures: A system description. Climbing and Walking Robots, 300.

Kim, S., Asbeck, A., Cutkosky, M., & Provancher, W. (2005). SpinybotII: climbing hard walls with compliant microspines. Advanced Robotics, 2005. ICAR '05, Proceedings, 12th International Conference (pp. 601–606).

Kim, S., & Cutkosky, M. (2008). Design and fabrication of multimaterial structures for bio-insired robots. Journal of the Royal Society, 18.

Kissel, J., & Krueger, F. (1987). The organic component in dust from comet Halley as measured by the PUMA mass spectrometer on board Vega 1. Nature, 326, 755–760.

Kleine, T., Touboul, M., Bourdon, B., Nimmo, F., Mezger, K., Palme, H., Jacobsen, S., Yin, Q., & Halliday, A. (2009). Hf-w chronology of the accretion and early evolution of asteroids and terrestrial planets. Geochimica et Cosmochimica Acta, 73, 5150–5188.

Leveille, R., & Datta, S. (2010). Lava tubes and basaltic caves as astrobiological targets on Earth and Mars: A review. Planetary and Space Science, 58, 592–598.

Matthew, R., Lund, H., & Yoshida, K. (2010). A bio-inspired compliant claw for arboreal locomotion in microgravity environments. IEEE/SICE International Symposium on System Integration.

McEwen, A., Ojha, L., Dundas, C. et al. (2011). Seasonal flows on warm martian slopes. Science, 333, 740–743.

Merz, R., Prinz, F., Ramaswami, K., Terk, M., & Weiss, L. (1994). Shape deposition manufacturing. Solid Freeform Fabrication Symposium.

Nesnas, I., Manterola, R., Edlund, J., & Burdick, J. (2008). Axel mobility platform for steep terrain excursions and sampling on planetary surfaces. IEEE Aerospace Conference.

Obama, B. (2010). Speech at Kennedy Space Center.

Okon, A. (2010). Mars science laboratory drill. 40th Aerospace Mechanisms Symposium.

Parness, A. (2013). youtube.com/watch?v=4JJfIEK0Adw.

Parness, A., & DiscoveryChannel (2009). Gecko super suit. Television Episode: Prototype This! Episode 11.

Parness, A., Frost, M., Boston, P., & Cutkosky, M. (2012). Rock climbing robot for exploration and sample acquisition at lava tubes, steep slopes, and cliff walls. LPI Conference on Mars Concepts.

Parness, A., Frost, M., Thatte, N., & King, J. (2012a). Gravity-independent mobility and drilling on natural rock using microspines. IEEE ICRA.

Parness, A., Frost, M., Thatte, N., & King, J. (2012b). Video demonstration of gravity-independent mobility and drilling on natural rock using microspines. IEEE ICRA.

Saito, J., Miyamoto, H., Nakamura, R. et al. (2006). Detailed images of asteroid 25143 Itokawa from Hayabusa. Science, 312, 1341–1344.

Sandford, S., Aleon, J., Alexander, C. et al. (2006). Organics captured from comet 81P/Wild2 by the Stardust spacecraft. Science, 314, 1720–1724.

Shapiro, I., A'Hearn, M., Vilas, F. et al. (2010). Defending planet Earth: Near-Earth object surveys and hazard mitigation strategies. National Academy Press.

Spenko, M., Cutkosky, M., Majidi, C., Fearing, R., Groff, R., & Autumn, K. (2006). Foot design and integration for bioinspired climbing robots. In Defense and Security Symposium (pp. 623019–623019). International Society for Optics and Photonics.

Spenko, M., Haynes, G., Saunders, J., Cutkosky, M., & Rizzi, A. (2008). Biologically inspired climbing with a hexapedal robot. Journal of Field Robotics.

Squyres, S. (2011). Vision and voyages for planetary science in the decade 2013–2022. National Research Council Publications.

Squyres, S., Knoll, A., Arvidson, R. et al. (2009). Exploration of Victoria Crater by the Mars rover Opportunity. Science, 324, 1058–1061.

Veverka, J., Farquhar, B., Robinson, M. et al. (2001). The landing of the near-shoemaker spacecraft on on asteroid 433 Eros. Nature, 413, 390–393.

Yoshida, K., Maruki, T., & Yano, H. (2002). A novel strategy for asteroid exploration with a surface robot. 2nd World Space Congress, 34th COSPAR Scientific Assembly.

Yoshida, K., Nishimaki, Y., Maruki, T., Kubota, T., & Yano, H. (2003). Sampling and surface exploration strategies in muses-c and future asteroid missions. 7th International Symposium on Artificial Intelligence and Robotics and Automation in Space.

Younse, P., Collins, C., & Backes, P. (2010). A sample handling, encapsulation, and containerization subsystem concept for Mars sample caching missions. International Planetary Probe Workshop.

Zacny, K., Bar-Cohen, Y., Brennan, M., Briggs, G., Cooper, G. et al. (2008). Drilling systems for extraterrestrial subsurface exploration. Astrobiology, 8.

Zinner, E. (2003). Presolar grains. Treatise on Geochemistry, Volume 1: Meteorites, Comets, and Planets (pp. 17–39).